What historical landfast ice observations tell us about projected ice conditions in Arctic Archipelagoes and marginal seas under anthropogenic forcing

Frédéric Laliberté[1], Stephen. E. L. Howell[1], Jean-François Lemieux[2], Frédéric Dupont[3] and Ji Lei[3]

[1]Climate Research Division, Environment and Climate Change Canada, Toronto, Ontario, Canada

[2]Recherche en Prévision Numérique Environnementale, Environnement et Changement Climatique Canada, Dorval, Québec, Canada

[3]Service Météorologique Canadien, Environnement et Changement Climatique Canada, Dorval, Québec, Canada

Correspondence to: Frédéric Laliberté (laliberte.frederic@gmail.com)

Abstract. Arctic landfast ice extent and duration from observations, ice assimilations, ocean re-analyses and coupled models are examined. From observations and assimilations, it is shown that in areas where landfast ice conditions last more than 5 months the first-year ice grows typically to more than 2 m and is rarely less than 1 m. The observed spatial distribution of landfast ice closely matches assimilation products but less so for ocean re-analyses and coupled models. Although models generally struggle to represent the landfast ice necessary to emulate the observed import/export of sea ice in regions favourable to landfast ice conditions, some do exhibit both a realistic climatology and a realistic decline of landfast ice extent under an anthropogenic forcing scenario. In these more realistic simulations, projections show that an extensive landfast ice cover should remain for at least 5 months of the year well until the end of the 21st century. This is in stark contrast with the simulations that have an unrealistic emulation of landfast ice conditions. In these simulations, slow and packed ice conditions shrink markedly over the same period. In all simulations and in areas with landast ice that last more than 5 months, the end-of-winter sea ice thickness remains between 1 m and 2 m well beyond the second half of the century. It is concluded that in the current generation of climate models, projections of winter sea ice conditions in the Canadian Arctic Archipelago and the Laptev Sea are overly sensitive to the representation of landfast ice conditions and that ongoing development in landfast ice parametrization will likely better constrain these projections.

1 Introduction

Sea ice that is immobile because it is attached to land is termed "landfast". In shallow coastal regions, large pressure ridges can get anchored at the sea floor. These grounded ridges might then act as anchor points to stabilize and maintain a landfast ice cover [Mahoney et al., 2007]. However, landfast ice is also present in some coastal regions that are too deep for pressure ridges to become grounded. In this case, the ice can stay in place due to the lateral propagation of internal ice stresses that originate where the ice is in contact with the shore. Sea ice typically becomes landfast if its keel extends all the way to the sea floor or if ice stresses cannot overcome lateral friction at the coastline [Barry et al., 1979]. Most (but not all) landfast ice melts or becomes mobile each summer. Multi-year landfast ice (also termed an "ice-plug") is rare but it is known to occur within the Nansen Sound and Sverdrup Channels regions within the Canadian Arctic Archipelago (CAA) [Serson, 1972; 1974]. These ice-plugs were once a prominent feature within the CAA from the 1960s (Nansen Sound) and 1970s (Sverdrup Channel) up until they were both removed during the anomalously warm summer of 1998 and have since rarely re-formed [Alt et al., 2006]. The disappearance of multi-year landfast ice is coincident with a decline in pan-Arctic landfast ice extent of approximately 7% decade-1 from 1976 to 2007 [Yu et al., 2013]. Landfast ice has not only shrunk in extent but has also thinned. While few long-term records of sea ice thickness exist, they all show a thinning of springtime landfast ice. The largest declines are generally found in the Barents Sea at 11 cm decade-1 [Gerland et al., 2008]. Along the Russian coast and in the CAA, the thinning has generally been less pronounced and is on average less than 5 cm decade-1 [Polyakov et al., 2010 for Russia, Howell et al., 2016 for Canada].

Landfast ice is immobile and, therefore, its maximum ice thickness is primarily driven by thermodynamics from air temperature and the timing and amount of snowfall during the growth period [Brown and Cote, 1992]. Because it isolates thermodynamics from import/export of sea ice, landfast ice is a convenient bellwether of the effect of anthropogenic forcing on the Arctic environment. This convenience has motivated several studies that investigated the sensitivity of landfast ice to anthropogenic forcing in both one-dimensional thermodynamic models [Flato and Brown, 1996; Dumas et al., 2006] and CAA-focused regional three-dimensional ice-ocean coupled models [e.g. Sou and Flato, 2009]. Since the Sou and Flato [2009] study, several high resolution global ocean and sea ice models have become available, thus making it possible to study the coupled response of landfast ice to anthropogenic forcing. These models include the Community Earth System Model Large Ensemble (CESM-LE), coupled climate models from the Coupled Model Intercomparison Project phase 5 (CMIP5) and from the Ocean Reanalysis Intercomparison Project (ORA-IP). Howell et al., [2016] provide a preliminary in-vestigation of the aforementioned climate models within the CAA over a 50+ year record from 1957-2014 and found that they provide a reasonable climatology but trends were unrealistic compared to observations.

54 In this study, we provide a more comprehensive investigation into variability of landfast ice extent and thickness from the

55 current generation of climate models for the Arctic-wide domain and also evaluate their response to anthropogenic forcing.

56 As climate models do not output a dedicated landfast ice variable and as the ice velocity does not completely vanish when

57 landfast ice is simulated, we first develop an approach to characterize landfast ice. We then describe the historical evolution

58 of landfast ice extent and springtime landfast ice thickness as well as their future projections in models. Finally, we compare

59 the coupled model simulations with our own pan-Arctic ice-ocean simulations.

2 Data Description

2.1 Observations

62 One of the longest records of landfast ice thickness and duration comes from several coastal stations throughout Canada that

63 date back to the late 1940s, depending on the location. The dataset is available online at the Canadian Ice Service (CIS) web

64 site (http://www.ec.gc.ca/glaces-ice/, see Archive followed by Ice Thickness Data). The thickness measurements are usually

65 performed weekly from freeze-up to breakup, as long as it is safe to walk on the ice. For these reasons, the landfast ice dura-

66 tion at these stations, measured as the number of weeks with measurements, is always biased on the shorter side, possibly by

67 a few weeks. From these station records, we selected the four sites in the CAA that had continuous records up to 2015: Alert,

68 Eureka, Resolute and Cambridge Bay. From these weekly records available from 1960 to 2015, we extracted the landfast ice

69 duration and springtime landfast ice thickness. A thorough analysis of these quantities as derived from these records was pre-

70 sented initially by Brown and Cote [1992] from 1957-1989 and recently updated to 2014 by Howell et al. [2016].

71 For additional ice thickness information we use ice thickness surveys in landfast regions of the CAA carried out by means of

72 airborne electromagnetic induction (AEM) sounding in 2011 and 2015 previously described in Haas and Howell [2015].

73 These surveys were averaged on a 25 km EASE 2.0 grid and are shown in Figure S1 of the supplementary online material.

74 We also use weekly ice thicknesses retrieved from CryoSat-2 / SMOS in netCDF format for the years 2010-2016, obtained

75 from data.scienceportal.de and remapped using a nearest-neighbour remapping to a 25 km EASE 2.0 grid. The resulting win-

76 ter maximum sea ice thicknesses are shown in Figure S2 of the supplementary online material.

77 In order to spatially map landfast ice we use the National Ice Center (NIC) ice charts products from the NSIDC (dataset ID

78 G02172) and ice charts from the Canadian Ice Service Digital Archive (CISDA). The NIC ice charts are available from 1972

79 to 2007 but we restrict the time period to 1980-2007 to be consistent with CISDA. Indeed, the CISDA provide ice informa-

80 tion before 1980 but landfast ice was not explicitly classified. We refer readers to Tivy et al. [2011] (CISDA) and Yu et al.

81 [2014] (NIC) for in-depth descriptions of ice chart data and their validity as a climate record. Following Galley et al. [2010],

82 who also used the CIS ice chart data to map landfast ice, we consider grid cells with sea ice concentration of 10/10ths to be

83 landfast. We defined pan-Arctic landfast extent using the NIC ice charts (given their larger spatial domain) as the regions

84 that are covered by landfast ice for at least one month in the climatology. Both the NIC and CISDA ice charts were con-

85 verted from shape files to a 0.25° latitude-longitude grid and then converted using a nearest-neighbor remapping to a 25 km

86 Equal-Area Scalable Earth (EASE) 2.0 grid. We compute the number of months (equivalent to "percent of the year" in Gal-

87 ley et al.) during which each grid cell was landfast for each time period from September to August.

88 **2.2 Models**

89 Climate simulations and reanalyses do not provide a variable that explicitly characterizes landfast ice conditions. This makes

90 it challenging to verify how it emulates landfast ice conditions as compared to observations. To circumvent this limitation,

91 we use daily sea ice thickness (hereafter, sit), sea ice concentration (hereafter, sic) and sea ice velocities (hereafter, usi and

92 vsi) to synthetically characterize landfast sea ice conditions using the following procedure:

93 1. On the original model grid, we set the land mask to its nearest neighbor and remap using a nearest neighbor remapping

94   usi, vsi and sit to the sic native grid. Finally, we use a nearest neighbor remapping to put all variables on a EASE 2.0

95   grid.

96 2. The sea ice speed (hereafter, speedsi) is computed from usi and vsi on this new grid.

97 3. Daily speedsi, sit and sic are averaged to weekly means.

98 4. A grid cell is identified as having "packed ice" if the remapped weekly-mean sic is larger than 85%.

99 5. A grid cell is identified as having "slow ice" if the remapped weekly-mean speedsi is less than 1 cm s-1 (~1 km day-1).

100 6. Slow, packed ice is used as a proxy for landfast ice.

101

102 At each grid cell we then compute the number of months in each year with slow, packed ice. Using slow, packed ice is repre-
103 sentative because we are interested in one specific aspect of landfast ice: the fact that its growth is primarily driven by ther-
104 modynamics and not by the import/export of sea ice. This procedure is used with the Pan-Arctic Ice-Ocean Modeling and
105 Assimilation System (PIOMAS) [Zhang and Rothrock, 2003], a subset of the highest resolution models [see Table 3, Storto
106 et al., 2011; Forget et al. 2015; Haines et al., 2014, Zuo et al., 2015; Masina et al., 2015] from the ORA-IP [Balsameda et al.,
107 2015; Chevallier et al., 2016]. Finally, we use the CESM-LE and CMIP5 models to analyze climatological landfast ice extent
108 and thicknesses. Some ORA-IP models (ORAP5.0, UR025.4) do not provide daily output. For these models, monthly data
109 was first interpolated to daily frequency and from then on the analysis was performed using the procedure described above.
110 It should be noted that sea ice velocities are not provided by all models and only for a few simulations, constraining the
111 scope of the intercomparison presented here (see available models in Table 1). The data for this study was retrieved from the
112 ESGF using the cdb_query tool (github.com/cdb_query). Finally, the 1980-2005 Historical experiment followed by the
113 2006-2015 Representative Concentration Pathway 8.5 (RCP85) experiment [Taylor et al. 2012] are used with daily sea ice
114 velocities, thickness and concentration.

115

116 In the summer, the sea ice concentration drops below 100% for some models but it stills remains relatively high throughout
117 the melt season. In these models (e.g. NorESM1 and ACCESS1.0), the reduction in summer ice concentration is not associ-
118 ated with increased sea ice speed (i.e. close to 0 correlation between the two variables over a year), unlike in the PIOMAS
119 product where a strong anti-correlation between the two variables can be measured. This suggests that these models may in-
120 deed have an ice concentration below 100% during the summer but the import/export of sea ice remains quite limited be-
121 cause the packed ice never becomes mobile enough in narrow channels, particularly within the CAA. As a result, one must
122 thus allow for some flexibility in the definition of packed ice in modelled products and a number below 100% needs to be
123 chosen as a cutoff. Here, we have chosen 85% because i) it represents landfast ice that ice grows according to thermody-
124 namics and not because of export/import and ii) it is widely accepted that in historical observational products a 15% uncer-
125 tainty in sea ice concentration is to be expected and since we are using historical observation products in our comparison, we
126 argue that the same 15% uncertainty should be used when assessing model behaviour. We acknowledge that by using an
127 85% ice concentration to define packed ice, the lead fraction could be large at the boundary of the slow, packed ice, due to
128 the proximity of mobile ice. In these regions, the argument presented above might break down. In this work, we will primar-
129 ily focus on archipelagoes and marginals seas where this is not an issue. It is however important to keep in mind that for ap-
130 plications that focus on those boundary regions, this criterion might be too lenient.

131

132   The models listed above do not represent the grounding of pressure ridges. Hence, they are not expected to perform well in

133   regions where grounding is known to be an important mechanism for the formation and stabilization of a landfast ice cover.

134   Observations show that grounding is important in the Laptev Sea [Haas et al., 2005, Selyuzhenok et al., 2017], in the Beau-

135   fort Sea [Mahoney et al., 2007] and in the Chukchi Sea [Mahoney et al., 2014]. Nevertheless, these models can simulate

136   landfast ice in some regions because the models dynamics take into account the aforementioned mechanical interactions. For

137   most of these sea ice models, ice interactions are represented by a viscous-plastic rheology with an elliptical yield curve [Hi-

138   bler, 1979].

139

140   Recently, a basal stress parameterization representing the effect of grounding was developed [Lemieux et al. 2015]. This pa-

141   rameterization calculates, based on simulated ice conditions, the largest ridge(s) at each grid point. When these subgrid scale

142   ridge(s) are able to reach the sea floor, a basal (or seabed) stress term is added to the sea ice momentum equation. This

143   grounding scheme clearly improves the simulation of landfast ice in regions such as the Alaskan coast, the Laptev Sea and

144   the East Siberian Sea. However, in deeper regions such as the Kara Sea, Lemieux et al. (2015) pointed out that their model

145   systematically underestimates the area of landfast. As the grounding scheme is less active in these deeper regions, Lemieux

146   et al. 2016 modified the viscous-plastic rheology to promote ice arching.

147

148   Following the work of Lemieux et al. 2016, we conducted simulations that combined the grounding scheme and a modified

149   viscous-plastic rheology. We used the optimal parameters $k1=8$ and $k2=15$ Nm-3 for the grounding scheme [Lemieux et al.

150   2015]. Given a certain mean thickness in a grid cell and a concentration, the grounding scheme determines whether the pa-

151   rameterized ridges reach the seafloor or not (which depends on k1) and defines the maximum seabed stress that can be sus-

152   tained by the grounded ridges (which is proportional to k2). As opposed to the standard elliptical yield curve, the ellipse as-

153   pect ratio is set to 1.5 (instead of 2) and a small amount of isotropic tensile strength is used (kt=0.05).

154

155   For these simulations, we used the ocean model NEMO version 3.1 and the sea ice model CICE version 4.0 with code modi-

156   fications to include the grounding scheme and to add tensile strength [Lemieux et al. 2016]. Our 0.25˚ grid is a subset of the

157   global ORCA mesh. It covers the Arctic Ocean, the North Atlantic and the North Pacific. This ice-ocean prediction system,

158   that includes tides, was developed as part of the CONCEPTS (Canadian Operational Network of Coupled Environmental

159   PredicTion Systems) initiative. We refer to our 0.25˚ model setup and simulations as CREG025 (CONCEPTS-regional

160   0.25˚).

161   Note that while adding the tides to our ice-ocean prediction systems, we found that unrealistic sea thicknesses developed in

162   late winter in tidally active regions (e.g. Foxe Basin). To mitigate this problem, the Hibler 1979 ice strength parameterization

163   is used as opposed to the default Rothrock 1975 formulation. The ice strength parameter P* was set to 27.5 kNm-2 for our

164   CREG025 simulation.

165 The sea ice model was initialized with sea ice thicknesses and concentrations from the GLORYS2V1 ocean reanalyses. The

166 ocean model was initialized by the World Ocean Atlas (WOA13) climatology and forced at open boundaries by GLO-

167 RYS2V3 (Ferry et al. 2010; Chevallier et al., 2017). A spin up from October 2001 to September 2004 was performed. Free

168 runs (no assimilation) are then restarted from the fields in September 2004 and conducted up to the end of 2010. The simula-

169 tion was forced by 33 km Environment Canada atmospheric reforecasts [Smith et al. 2014].

170 **3 Results**

171 **3.1 Landfast ice duration and thickness**

172 The CAA is almost entirely covered by landfast ice for up to 8-months of the year (i.e. November to July) [Canadian Ice Ser-

173 vice, 2011] and is therefore a useful region to begin evaluating model representation of landfast ice duration and thickness.

174 Figure 1 illustrates the relationship between landfast ice thickness and duration within the CAA for the observed datasets

175 (e.g. CryoSat-2, AEM and in situ) in addition to PIOMAS and CREG025. When combining these heterogeneous data

176 sources, a general picture of their representativeness of ice thickness over landfast ice duration emerges. Based on in situ ob-

177 servations landfast ice within the CAA lasts from 4 to ~9 months grows to ~2 m which is in agreement with previous studies

178 [e.g. Brown and Cote, 1992; Canadian Ice Service, 2011; Howell et al., 2016]. For PIOMAS, CREG025 and CryoSat-2 ice

179 thickness standard deviations are close to the variability observed at the in situ locations. However, very thick ice upwards of

180 ~4 m is encountered at the 95th percentile in both the CryoSat-2 and the PIOMAS data when the landfast ice lasts for more

181 than 9 months. These very stable and thick landfast conditions are the result of large multi-year ice floes, thus increasing the

182 average ice thickness. It has long been known that MYI forms in situ within the CAA and very thick MYI from the Arctic

183 Ocean is also advected into the region [e.g. Melling, 2002] which is evident from the airborne EM measurements thickness

184 values [Haas and Howell, 2015]. This mix of ice-types makes it challenging for models to represent ice thickness within the

185 CAA but overall, they are in reasonable agreement with observations.

186

187 **3.2. Geographical distribution and climatology**

188   The spatial distribution of annual landfast duration from observations (CIS and NIC), PIOMAS and selected ocean re-analy-

189   sis models is shown in Figure 2. Both ice charts products (CIS and NIC) show a similar landfast ice extent and duration in

190   the CAA (Figure 2a-b). This landfast ice extent is also very similar in the two ice chart products over their regions of overlap

191   (Figure 2a-b, magenta curve). In PIOMAS, the duration of slow and packed ice conditions, compares relatively well to the

192   overall landfast extent and duration in the ice chart products (Figure 2c). There is however, too much of the slow and packed

193   ice in the Beaufort Sea but too little in the Laptev and Kara Seas. Most ocean re-analysis products have a suitable representa-

194   tion of slow, packed ice conditions in the CAA, the notable exception being CGLORS and UR025.4 (not shown). In the

195   CGLORS case, the ice component appears to still be in spin-up at the beginning of the integration period because there is an

196   unphysical interannual variability in the first few years of the simulation and therefore results should not be expected to con-

197   form to observations. In the UR025.4 case, winter ice is packed but is too mobile in the Parry Channel and the M'Clintock.

198   The spatial distribution of annual landfast ice duration in CMIP5 models with higher resolution is illustrated in Figure 3b-h.

199   These models exhibit a reasonable slow, packed ice extent and duration but it is mostly confined to the CAA (Fig. 3b-h). The

200   exception is the MRI-ESM1 (and applies to the other models from the MRI) that simulate slow, packed ice conditions year-

201   round across the Arctic (not shown). This is likely due to its sea ice being modeled as a simple viscous fluid, without a so-

202   phisticated rheology. Compared to the NIC analyses, all the CMIP5 models and reanalyses do not have enough months of

203   landfast ice on the Russian coast. GFDL-ESM2G , CESM-LE and PIOMAS are the ones that provide the best landfast ice

204   simulation in the Laptev, Kara and East Siberian Seas (Figure 2c; Figure 3d,f). Another important feature of the import/ex-

205   port of sea ice in coupled models (ACCESS 1.0, CESM-LE, GFDL-ESM2G) seems to be the tendency of many of them to

206   emulate year-round or close to year-round landfast ice in the Parry Channel regions of the CAA (Figure 3d,f, ACCESS 1.0

207   not shown). This is peculiar since this would mean that ice likely takes years to transit through the Parry Channel, allowing

208   thermodynamic forcing to create very thick ice in a region. Note that in the remaining models, the MIROC5 and MPI-ESM-

209   MR both emulate too short of a landfast ice duration in the Parry Channel (Figure 3c,e).

210

211   **3.3. Trends in landfast ice duration**

212 The largest observed negative trends in landfast ice duration of up to 1 month decade-1 is found primarily in the East
213 Siberian Sea but a general negative trend is located across the Arctic (Fig. 4a-b) as also reported by Yu et al. [2014]. In the
214 CAA, trends are larger in the NIC ice charts but both the CIS and NIC show relatively weak duration declines in the Parry
215 Channel and the M'Clintock. These relatively small trends are in stark contrast with the very large trends almost everywhere
216 in the CAA in the PIOMAS simulations. For CGLORS, the model whose sea ice is still in spinup, there is a large positive in-
217 crease in slow, packed ice duration (not shown). Such increases are also seen in the Beaufort Sea in the GLORYS2V3 re-
218 analysis indicating that towards the end of the reanalysis the Beaufort Sea is covered by slow, packed ice for a few months
219 per year (Figure 4f). This is in complete disagreement with observations and mandates that extra care be taken when using
220 this product to analyze the import/export of sea ice in the Beaufort Sea. In summary, re-analysis products appear to have a
221 particularly difficult time reproducing the long-term stability of the slow, packed ice distribution, suggesting that targeted ef-
222 forts to improve this aspect of their import/export of sea ice are likely necessary.
223 CMIP5 models sea ice simulations (except the MRI models for the reason explained above), on the other hand, fare rela-
224 tively well at representing negative trends in landfast ice duration when compared to observations (Figure 5). Most models
225 tend to show an enhanced disappearance of slow, packed conditions along the Beaufort Sea edge of the CAA and declines
226 that are in general agreements with observation in the Parry Channel. One exception is the CESM-LE where some of year-
227 round slow, packed ice conditions are not declining over the 1980-2015 period (Figure 5d). The models with less slow,
228 packed ice than in observations, MIROC5 and MPI-ESM-MR, show relatively strong declines that, if they continued, would
229 indicate an almost complete disappearance of slow, packed ice by mid-21st century.
230

3.4. Regional evaluation of landfast ice extent and thickness

232 We now take a closer regional examination at landfast ice extent in the CAA, Northwest Passage (Parry Channel route) and
233 Laptev Seas. These regions are expected to experience increases in shipping activity from the mid to late-21st century ac-
234 cording to model simulations [Smith and Stephenson, 2013; Melia et al., 2016]. Instead of using an absolute measure of ex-
235 tent, we report extent as a fraction of the ocean surface within the bounds of the NIC 1 month duration landfast ice extent cli-
236 matology (magenta line in Figure 2b). This approach is necessary to appropriately compare observations to models that rep-
237 resent the islands and channels of the CAA differently.

238 Over the 1980-2015 time period, landfast ice extent has declined dramatically for durations longer than 5 months with a
239 marked decline in the extent of landfast ice with a 7 to 8 months duration within the Northwest Passage (Figure 6). What is
240 however striking is how the extent of landfast ice extent with duration of 5 months or less has been mostly constant over the
241 last 35 years (Figure 6). It is because of this observation that that we have not included a trend analysis in Figure 6. If the
242 trend in landfast area depends so strongly on landfast ice duration, it would probably be misleading to attribute a hard num-
243 ber to the decline in landfast ice. If sea ice-albedo feedback is an important player in recent sea ice decline [e.g. Perovich et
244 al., 2007] then it is not entirely surprising that during the polar night landfast ice conditions re-establish themselves year after
245 year even in the context of rapid Arctic warming. Finally, it is also worth noting that Figure 6a indicates that the small
246 amounts of multi-year landfast ice within the CAA have virtually disappeared in recent years (i.e. the 11 months line is at 0
247 since 2002) consistent with Alt et al., [2009].
248 Landfast ice extent in the CAA and Northwest Passage is well represented in the PIOMAS data assimilation product as it
249 compares well with the CIS and NIC ice chart products although, the NIC product does exhibit stronger interannual variabil-
250 ity (Fig. 7a-b). In the Laptev Sea, PIOMAS clearly underestimates the area of landfast ice when compared to the NIC ice
251 charts (Figure 7c). This is likely due to the fact that PIOMAS does not represent the effect of grounding, an important mech-
252 anism for the formation and stability of the Laptev Sea landfast ice cover [Selyuzhenok et al., in press]. Despite this too
253 small area of landfast ice in the Laptev Sea, PIOMAS exhibits a decline of ~25% of the landfast extent over the last 35 years
254 which is consistent with the one from the NIC ice charts.
255 Comparing current (1980-2015) to projected (2070-2080) landfast ice extent from CMIP5 in these regions reveals consider-
256 able changes which are summarized in Table 1. The seven models with the lowest extent of 1979-2015 CAA slow, packed
257 ice (ACCESS1.0, ACCESS1.3, BCC-CSM1.1(m), GFDL-CM3, MIROC5, MPI-ESM-LR, MPI-ESM-MR) lose most of it by
258 2070-2080 while the four models with a large extent of 1979-2015 CAA slow, packed ice (CESM-LE, GFDL-ESM2G,
259 GFDL-ESM2M, NorESM1-M) retain most of it by 2070-2080. As mentioned earlier, two models have unrealistic behavior
260 (MIR-ESM, MRI-CGCM3) because their sea ice model is based on a simple perfect fluid.
261 Looking specifically in the CAA, current conditions (Figure 8a, black) indicate that the CMIP5 distribution is tri-modal: one
262 mode has an extent comparable to observations (at 0.6 to 0.8 of NIC extent), a second mode has a much lower extent (at 0.2 -
263 0.6 of NIC extent) and a third mode has an extent that covers most of the area (~1.0 of NIC extent). In the CAA, this tri-
264 modal distribution yields to a bi-modal distribution in 2070-2080 projections (Figure 8a, yellow): one mode still has an ex-
265 tent comparable to observations and a second mode has virtually no 5-month landfast ice extent left. In the Northwest Pas-
266 sage, the story is much simpler (Figure 8b). All considered models are entirely covered with slow, packed ice conditions at
267 least 5 months every year for their historical simulations but in 2070-2080 projections about half become devoid of it while
268 the other half retain their historical conditions. This highlights difficulty of projecting how the import/export of sea ice will
269 react to anthropogenic forcing in the narrow channels of the CAA. Finally, in the Laptev Sea, almost all considered models
270 have little slow, packed ice extent now and by 2070-2080 (Figure 8c).

271 The picture is generally clearer for the CESM-LE. In that model, the CAA and the Northwest Passage has slow, packed ice
272 comparable to observation (Figure 8d-e). In the projection, the CAA is expected to lose only 0.2 of its slow, packed ice cov-
273 erage and almost none in the Northwest Passage. In the Laptev Sea, the CESM-LE is only performing marginally better that
274 the CMIP5 multi-model ensemble and the projection shows the complete disappearance of 5-month slow, packed ice by
275 2070-2080 (Figure 8f).

276 When we look at ice thickness, models show a wide range of ice thicknesses over landfast ice during the 1980-2015 period
277 for all regions (Figure 9a-c). However, for the 2070-2080 period they are essentially in agreement indicating that in all three
278 regions considered landfast ice thickness is found to grow between 1 and 2 meters over the cold season (Fig. 9a-c). More-
279 over, the projections indicate about a 0.5 m decrease in landfast ice thickness towards the end of the 21st century. A similar
280 growth range is apparent when just looking at the CESM-LE but there is however a larger magnitude of projected thickness
281 decreases towards the end of the 21st century (Figure 9d-f).

282

283 **3.5. Ice-ocean simulations with landfast ice parameterizations**

284 The results we have presented so far have been focused on high-resolution observational datasets, 25 km resolution reanaly-
285 ses and coarser climate models. From these different data sources we were able to demonstrate the capabilities and limita-
286 tions at emulating landfast ice conditions of models of the current generation. In the remainder of this section, we will look
287 at our CREG025 6 year simulations and see the benefits of using landfast ice parameterizations.

288

289 As evident in Figure 10, the CREG025 simulations show a quite accurate representation of landfast ice duration in the
290 Laptev Sea, the East Siberian Sea and along the Alaskan Coast where grounding is crucial for simulating landfast ice
291 [Lemieux et al., 2015] . The overestimation of landfast ice North of the CAA is likely a consequence of our imperfect crite-
292 rion for determining whether the ice is landfast or not (slow drifting ice for a NIC analyst can be identified as landfast in our
293 study).

294 Overall, in the CAA, the CREG025 landfast ice duration is in good agreement with the ones of the NIC and CIS (Figure 2a-
295 b). In both NIC and CIS products, the duration of landfast ice is small in tidally active regions such as the Gulf of Boothia,
296 Prince Regent Inlet, Lancaster Sound and Foxe Basin. In accordance with observations, the CREG025 simulation (which in-
297 cludes explicit tides), exhibits mobile ice in these regions throughout the winter (Figure 10b). However, CREG025 underes-
298 timates the landfast ice duration in Barrow Strait and north of M'Clintock.

299 We are currently doing a thorough investigation of the impact of tides (and the mechanisms involved) on simulated landfast
300 ice. This will be the subject of a future publication. Preliminary results suggest that including tides is crucial to properly sim-
301 ulate landfast ice in certains regions of the CAA. We speculate that the fact that many models (e.g. GFDL-ESM2G , CESM-
302 LE, PIOMAS) presented in this paper, overestimate landfast ice in parts of the CAA (e.g. Gulf of Boothia and Prince Regent
303 Inlet) is due to the absence of tides in their simulations.

304 Looking at time series of 5 month landfast ice extent, the CREG025 simulation follows observations very closely in the
305 CAA and Laptev Sea (Figure 7a,c). In the Northwest Passage, however, the CREG025 simulation leads to too litlle landfast
306 ice (again due to the underestimation of landfast ice in Barrow Strait and north of M'Clintock). This could be due to the fact
307 that our CREG025 simulation seems to have ice thinner (and therefore weaker) than observations (see Figure 1). Overall,
308 however, landfast ice extent in CREG025 is much more in line with observations in all three regions than most Earth system
309 models (shown in Figure 8).

310 **4. Discussion and conclusions**

311 In this study, we have compared the geographical distribution of landfast ice extent and duration in ocean reanalyses and
312 coupled climate models and to historical ice charts. To achieve this comparison, we have used slow, packed ice in models as
313 a proxy for landfast ice. Using this proxy we find that some current generation models provide a reasonable representation of
314 landfast ice conditions (e.g. PIOMAS, CESM-LE and GFDL-ESM2G) but others still have a hard time emulating landfast
315 ice particularly in the CAA and even more so in the Laptev Sea. Ice-ocean simulations with a grounding scheme and a modi-
316 fied rheology to promote arching indicate that these parameterizations have the capability to provide better projections for
317 seasonal economic activities in the Arctic. This is particularly important for reducing uncertainty in Arctic shipping projec-
318 tions based on model simulations from the current generation of models [e.g. Melia et al., 2016]

319 While many models do not emulate landfast ice accurately, their biases help explain why they project dramatic ice thickness
320 decreases in the CAA, decreases that are not supported by long observational records [Howell et al., 2016]. Specifically, in
321 regions with landfast ice, models tend to have very thick ice in their historical simulations that is very sensitive to anthro-
322 pogenic forcing. Later in the 21st century, once multi-year ice essentially disappears from the Arctic, the thickness distribu-
323 tion in models becomes much more in line with the thickness expected from a simple extrapolation of springtime landfast ice
324 thickness records of less than ~50 cm thinning over a century from typically ~2 m springtime thickness [Howell et al., 2016].
325 This is also observed in the projections analyzed in this study. Indeed, in the bulk of models and ensemble members in re-
326 gions where landfast ice lasts more than 5 months, the end-of-winter ice thickness remains between 1-2 m until the end of
327 21st century.

328 Finally, this analysis indicates that, although the sea ice cover is projected to shrink for many months and in many regions
329 [Laliberte et al., 2016], landfast ice should cover most of the CAA for much of the winter well past the mid-century. This
330 landfast ice should reasonably be expected to grow to 1.5 m each winter, meaning that by the time the ice breaks up, haz-
331 ardous ice floes should remain in the region for several weeks if not months every year. The presence of these hazardous ice
332 floes during the months with the most economic activity will likely have negative implications, especially for shipping in the
333 CAA. As a consequence, in order to deal with the annual replenishing of thick sea ice in the CAA, ships will probably re-
334 quire reinforced hull to ward off environmental disasters as the shipping season extends earlier in the season.

References

Alt, B., K. Wilson, and T. Carrieres (2006), A case study of old ice import and export through Peary and Sverdrup channels in the Canadian Arctic Archipelago: 1998-2004, Ann. Glaciol., 44, 329–338, doi:10.3189/172756406781811321.

Barry, R. G., R. E. Moritz, and J. C. Rogers (1979), The fast ice regimes of the Beaufort and Chukchi sea coasts, Alaska, Cold Reg. Sci. Technol., 1, 129– 152.

M.A. Balmaseda , F. Hernandez , A. Storto , M.D. Palmer , O. Alves , L. Shi , G.C. Smith , T. Toyoda , M. Valdivieso , B. Barnier , D. Behringer , T. Boyer , Y-S. Chang , G.A. Chepurin , N. Ferry , G. Forget , Y. Fujii , S. Good , S. Guinehut , K. Haines , Y. Ishikawa , S. Keeley , A. Köhl , T. Lee , M.J. Martin , S. Masina , S. Masuda , B. Meyssignac , K. Mogensen , L. Parent , K.A. Peterson , Y.M. Tang , Y. Yin , G. Vernieres , X. Wang , J. Waters , R. Wedd , O. Wang , Y. Xue , M. Cheval - lier , J-F. Lemieux , F. Dupont , T. Kuragano , M. Kamachi , T. Awaji , A. Caltabiano , K. Wilmer-Becker , F. Gaillard, The Ocean Reanalyses Intercomparison Project (ORA-IP), Journal of Operational Oceanography, Vol. 8, Iss. sup1, 2015, DOI:10.1080/1755876X.2015.1022329

Brown, R., and P. Cote (1992), Interannual variability of landfast ice thickness in the Canadian high arctic, 1950−89. Arctic, 45, 273–284.

Bromwich, D. H., A. B. Wilson, L. Bai, G. W. K. Moore, and P. Bauer, 2015: A comparison of the regional Arctic System Reanalysis and the global ERA-Interim Reanalysis for the Arctic. Q. J. R. Meteorol. Soc., doi: 10.1002/qj.2527

Bentsen, M., Bethke, I., Debernard, J. B., Iversen, T., Kirkevåg, A., Seland, Ø., Drange, H., Roelandt, C., Seierstad, I. A., Hoose, C., and Kristjánsson, J. E.: The Norwegian Earth System Model, NorESM1-M – Part 1: Description and basic evalu- ation of the physical climate, Geosci. Model Dev., 6, 687-720, doi:10.5194/gmd-6-687-2013, 2013.

Canadian Ice Service (2011), Sea Ice Climatic Atlas: Northern Canadian Waters 1981−2010, 995 pp., Ottawa.

Chevallier, M., Smith, G.C., Dupont, F., Lemieux, J.F., Forget, G., Fujii, Y., Hernandez, F., Msadek, R., Peterson, K.A., Storto, A. and Toyoda, T., 2017. Intercomparison of the Arctic sea ice cover in global ocean−sea ice reanalyses from the ORA-IP project. Climate Dynamics, 49(3), pp.1107-1136.

Dee DP, co-authors. 2011. The ERA-Interim reanalysis: configuration and performance of the data assimilation system. Q J R Meteorol Soc. 137: 553–597, doi:10.1002/qj.828.

368

369 Dumas, J. A., G. M. Flato, and R. D. Brown (2006), Future projections of landfast ice thickness and duration in the Canadian
370 Arctic. J. Climate, 19, 5175–5189.

371

372 Dupont, F., S. Higginson, R. Bourdalle-Badie, Y. Lu, F. Roy, G. C. Smith, J.-F. Lemieux, G. Garric, and F. Davidson
373 (2015), A high-resolution ocean and sea-ice modelling system for the Arctic and the North Atlantic oceans, Geosci. Model
374 Dev., 8, 1577–1594, doi:10.5194/gmd-8-1577-2015.

375

376 Druckenmiller, M. L., H. Eicken, M. A. Johnson, D. J. Pringle, and C. C. Williams (2009), Toward an integrated coastal sea-
377 ice observatory: System components and a case study at Barrow, Alaska. Cold Reg.Sci.Tech., 56, 61-72.

378

379 Ferry N, Parent L, Garric G, Barnier B, Jourdain NC (2010) Mercator global Eddy permitting ocean reanalysis GLO-
380 RYS1V1: description and results. Mercator-Ocean Q Newslett 36:15–27

381

382 Flato, G. M., and R. D. Brown (1996),Variability and climate sensitivity of landfast Arctic sea ice. J. Geophys. Res., 101
383 (C10), 25 767–25 777.

384

385 Forget, G., Campin, J.-M., Heimbach, P., Hill, C. N., Ponte, R. M., and Wunsch, C.: ECCO version 4: an integrated frame-
386 work for non-linear inverse modeling and global ocean state estimation, Geosci. Model Dev., 8, 3071-3104, doi:10.5194/
387 gmd-8-3071-2015, 2015.

388

389 Gerland, S., A. H. H. Renner, F. Godtliebsen, D. Divine, and T. B. Loyning (2008), Decrease of sea ice thickness at Hopen,
390 Barents Sea, during 1966-2007. Geophys. Res. Lett., 35, L06501.

391

392 Gough, W., A.S.Gagnon an H.P Lau (2004), Interannual variability of Hudson Bay Ice Thickness, Polar Geography, 28(3),
393 222-238.

394

395 Haines K, Valdivieso M, Zuo H, Stepanov VN. 2012. Transports and
396 budgets in a 1/4 ° global ocean reanalysis 1989–2010. Ocean Sci. 8(3): 333–344, doi:10.5194/os-8-333-2012.002/qj.2063.

397

398 Haas, C., and S. E. L. Howell (2015), Ice thickness in the Northwest Passage, Geophys. Res. Lett., 42,
399 doi:10.1002/2015GL065704

400

401 Haas, C., W. Dierking, T. Busche, and J. Hoelemann (2005), ENVISAT ASAR monitoring of polynya processes and sea ice
402 production in the Laptev Sea, Tech. rep., Alfred
403 Wegener Institute.

404

405 Hibler, W. D. (1979), A dynamic thermodynamic sea ice model, J. Phys. Oceanogr., 9,
406 815-846.

407

408 Howell, S. E. L., F. Laliberté, R. Kwok, C. Derksen and J. King (2016), Landfast ice thickness in the Canadian Arctic
409 Archipelago from Observations and Models, The Cryosphere, 10, doi:10.5194/tc-2016-71.

410

411 Jeffers, S., T. Agnew, B. Alt, R. De Abreu, and S. McCourt (2001), Investigating the anomalous sea ice conditions in the
412 Canadian High Arctic (Queen Elizabeth Islands) during the summer of 1998, Ann. Glaciol., 33, 507– 612.

413

414 Jeffries, M. O. and J. Richter-Menge, Eds. (2012), The Arctic [in State of the Climate in 2011], Bull. Amer. Meteor. Soc., 93
415 (7), S127-S148.

416

417 Jones, P.D., T.M.L. Wigley, C.K. Folland and D.E. Parker (1987), Spatial patterns in recent worldwide temperature trends.
418 Climate Monitor, 16(5): 175-185.

419

420 Jones, P.D., M. New, D.E. Parker, S. Martin, and I.G. Rigor (1999), Surface air temperature and its changes over the past
421 150 years, Rev. Geophys, 37(2),173–200.

422

423 König Beatty, C. and David M. Holland, 2010: Modeling landfast sea ice by adding tensile strength. J. Phys. Oceanogr., 40,
424 185–198. doi: http://dx.doi.org/10.1175/2009JPO4105.1

425

426 Kwok, R., and D. A. Rothrock (2009), Decline in Arctic sea ice thickness from submarine and ICESat records: 1958 – 2008,
427 Geophys. Res. Lett., 36, L15501, doi:10.1029/2009GL039035.

428

429 Kwok, R., G. F. Cunningham, M. Wensnahan, I. Rigor, H. J. Zwally, and D. Yi (2009), Thinning and volume loss of Arctic
430 sea ice: 2003-2008, J. Geophys. Res., doi:10.1029/2009JC005312.

431

432 Laxon S. W., K. A. Giles, A. L. Ridout, D. J. Wingham, R. Willatt, R. Cullen, R. Kwok, A. Schweiger, J. Zhang, C. Haas, S.
433 Hendricks, R. Krishfield, N. Kurtz, S. Farrell and M. Davidson (2013), CryoSat-2 estimates of Arctic sea ice thickness and
434 volume, Geophys. Res. Lett., 40, 732–737, doi:10.1002/grl.50193.

435

436 Lemieux, J.-F., L. B. Tremblay, F. Dupont, M. Plante, G. C. Smith, and D. Dumont (2015), A basal stress parameterization
437 for modeling landfast ice, J. Geophys. Res. Oceans, 120, 3157–3173, doi:10.1002/2014JC010678.

438

439 Lemieux, J.-F., F. Dupont, P. Blain, F. Roy, G. C. Smith, and G. M. Flato (2016), Improving the simulation of landfast ice
440 by combining tensile strength and a parameterization for grounded ridges, J. Geophys. Res. Oceans, 121, 3157–3173,
441 doi:10.1002/2016JC012006.

442

443

444 Masina, S. et al. An ensemble of eddy-permitting global ocean reanalyses from the MyOcean project. Clim. Dynam. 1–29
445 (2015). doi:10.1007/s00382-015-2728-5

446

447 Mahoney, A., H. Eicken, and L. Shapiro (2007), How fast is landfast sea ice? A study of the attachment and detachment of
448 nearshore ice at Barrow, Alaska. Cold Reg.Sci.Tech., 47, 233-255.

449

450 Melling, H. (2002), Sea ice of the northern Canadian Arctic Archipelago, J. Geophys. Res., 107(C11), 3181,
451 doi:10.1029/2001JC001102.

452

453 Melling, H., D. A. Riedel, and Z. Gedalof (2005), Trends in the draft and extent of seasonal pack ice, Canadian Beaufort
454 Sea, Geophys. Res. Lett., 32, L24501, doi:10.1029/s2005GL024483.

455

456 Melia, N., K. Haines, and E. Hawkins (2016), Sea ice decline and 21st century trans-Arctic shipping routes, Geophys. Res.
457 Lett., 43, 9720–9728, doi:10.1002/2016GL069315.

458

459 Ólason, E. Ö. (2012), Dynamical modeling of Kara Sea land-fast ice, PhD thesis, Univ. of Hamburg, Hamburg, Germany.

460

461 Perovich DK, Light B, Eicken H, Jones KF, Runciman K, Nghiem SV (2007) Increasing solar heating of theArcticOcean
462 and adjacent seas, 1979–2005: attribution and role in the ice-albedo feedback.Geophys Res Lett 34:L19505.
463 doi:10.1029/2007GL031480

464

465 Polyakov, I. V., et al. (2010), Arctic Ocean Warming Contributes to Reduced Polar Ice Cap. Journal of Physical Oceanogra-
466 phy, 40, 2743-2756

467

468 Rothrock, D. A. (1975), The energetics of the plastic deformation of pack ice by ridging,

469   Journal of Geophysical Research, 80 (33), 4514{4519.

470

471   Schweiger, A., R. Lindsay, J. Zhang, M. Steele, H. Stern, and R. Kwok (2011), Uncertainty in modeled Arctic sea ice vol-

472   ume, J. Geophys. Res., 116, C00D06, doi:10.1029/2011JC007084.

473

474   Selyuzhenok V, Mahoney A. R., Krumpen T., Castellani G., and Gerdes R. (2017). Mechanims of fast ice development in

475   the southeastern Laptev Sea: acase study for winter of 2007/08 and 2009/10. Polare Research (in press CHECK).

476

477   Serson, H.V. (1972), Investigations of a plug of multiyear old sea icein the mouth of Nansen Sound. Ottawa, Ont., Depart-

478   ment of National Defence, Canada. Defence Research Establishment Ottawa. (DREO Tech. Note 72-6.)

479

480   Serson, H.V. (1974), Sverdrup Channel. Ottawa, Ont., Department of National Defence, Canada. Defence Research Estab-

481   lishment Ottawa. (DREO Tech. Note 74-10.)

482

483   Smith, L. C., and S. R. Stephenson (2013), New Trans-Arctic shipping routes navigable by midcentury, Proc. Natl. Acad.

484   Sci. U.S.A., 13, 4871–4872, doi:10.1073/pnas.1214212110.

485

486   Smith, G. C., F. Roy, P. Mann, F. Dupont, B. Brasnett, J.-F. Lemieux, S. Laroche,

487   and S. B_elair (2014), A new atmospheric dataset for forcing ice-ocean models: evaluation of reforecasts using the Canadian

488   global deterministic prediction system, Q. J. R. Meteorol. Soc., 140 (680), 881{894, doi:10.1002/qj.2194.

489

490   Sou, T., and G. Flato (2009), Sea ice in the Canadian Arctic Archipelago: Modeling the past (1950-2004) and the future

491   (2041-60), J. Clim., 22, 2181–2198, doi:10.1175/2008JCLI2335.1

492   Stroeve, J. C., M. C. Serreze, M. M. Holland, J. E. Kay, J. Malanik, and A. P. Barrett (2011), The Arctic's rapidly shrinking

493   sea ice cover: A research synthesis, Clim. Change, 110(3-4), 1005–1027.

494

495   Storto A, Dobricic S, Masina S, Di Pietro P. 2011. Assimilating along-track altimetric observations through local hydrostatic

496   adjustments in a global ocean reanalysis system. Mon Wea Rev. 139: 738–754.

497

498   Taylor, K. E., R. J. Stouffer, and G. A. Meehl (2012), An overview of CMIP5 and the experiment design, Bull. Am. Meteo-

499   rol. Soc., 93, 485–498, doi:10.1175/BAMS-D-11-00094.1.

500

Tivy, A., S. E. L. Howell, B. Alt, S. McCourt, R. Chagnon, G. Crocker, T. Carrieres, and J. J. Yackel (2011), Trends and variability in summer sea ice cover in the Canadian Arctic based on the Canadian Ice Service Digital Archive, 1960–2008 and 1968–2008, J. Geophys. Res., 116, C03007, doi:10.1029/2009JC005855.

Vincent, L., X. Wang, E. Milewska, Hui Wan, F. Yang, and V. Swail (2012), A second generation of homogenized Canadian monthly surface air temperature for climate trend analysis. Journal of Geophysical Research, D18110, doi:10.1029/2012JD017859

Warren, S. G., I. G. Rigor, N. Untersteiner, V. F. Radionov, N. N. Bryazgin, Y. I. Aleksandrov, and R. Colony (1999), Snow depth on Arctic sea ice, J. Clim., 12, 1814– 1829.

Wilks, D. S., 2006: On "field significance" and the false discovery rate. J. Appl. Meteor. Climatol., 45, 1181–1189. doi: http://dx.doi.org/10.1175/JAM2404.1

Woo, M-K., and R. Heron (1989), Freeze-up and break-up of ice cover on small arctic lakes. In: Mackay, W.C., ed. Northern lakes and rivers. Edmonton: Boreal Institute for Northern Studies, 56-62.

Woo, M-K., R. Heron, P. Marsh, and P. Steer, (1983), Comparison of weather station snowfall with winter snow accumulation in High Arctic basins, Atmos.-Ocean, 21(3):312-325.

Yu, Y, H. Stern, C. Fowler, F. Fetterer, and J. Maslanik (2014), Interannual Variability of Arctic Landfast Ice between 1976 and 2007. J. Climate, 27, 227–243.
doi: http://dx.doi.org/10.1175/JCLI-D-13-00178.1

Zhang, J.L. and D.A. Rothrock, (2003), Modeling global sea ice with a thickness and enthalpy distribution model in generalized curvilinear coordinates, Mon. Weather Rev., 131, 845-861.

Zuo, H., Balmaseda, M. A. & Mogensen, K. (2015) The new eddy-permitting ORAP5 ocean reanalysis: description, evaluation and uncertainties in climate signals. Clim. Dynam. 1–21. doi:10.1007/s00382-015-2675-1

	Arctic		CAA		Northwest Passage		Laptev Sea	
	1979, 2016	2070, 2081	1979, 2016	2070, 2081	1979, 2016	2070, 2081	1979, 2016	2070, 2081
ACCESS1.0	0.33	0.10	0.70	0.15	1.00	0.11	0.02	0.00
ACCESS1.3	0.29	0.02	0.59	0.03	0.81	0.00	0.01	0.00
BCC-CSM1.1(m)	0.39	0.17	0.67	0.29	0.96	0.33	0.06	0.01
CESM-LE	0.52	0.42	0.91	0.68	1.00	0.98	0.10	0.03
GFDL-CM3	0.52	0.05	0.96	0.11	1.00	0.00	0.18	0.01
GFDL-ESM2G	0.63	0.40	0.99	0.67	1.00	0.71	0.29	0.12
GFDL-ESM2M	0.52	0.34	0.87	0.65	1.00	0.97	0.26	0.11
MIROC5	0.27	0.00	0.40	0.00	0.43	0.00	0.06	0.00
MPI-ESM-LR	0.29	0.07	0.44	0.10	0.59	0.05	0.02	0.00
MPI-ESM-MR	0.30	0.04	0.51	0.06	0.67	0.03	0.03	0.00
MRI-CGCM3	1.70	1.51	1.63	1.62	1.00	1.00	1.62	1.47
MRI-ESM1	1.69	1.41	1.63	1.61	1.00	1.00	1.62	1.36
NorESM1-M	0.57	0.49	0.93	0.69	1.00	1.00	0.01	0.00

Table 1. Fraction of NIC landfast ice extent (magenta line in Fig. 2**b**) covered by slow, packed ice with a duration of more than 5 month for different models, regions and periods.
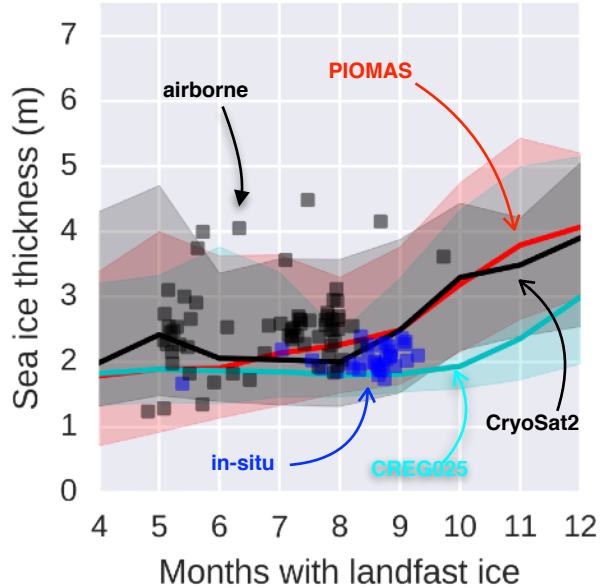
Figure 1. Canadian Arctic Archipelago (CAA) PIOMAS maximum ice thickness against landfast ice duration from Canadian Ice Service (CIS) Ice Charts over the 1980-2015 period (the mean is the thick red line, 95 one-sided percentile is the red shading). In black, the same is shown for CryoSat2 instead of PIOMAS over the period 2010-2015 (see Fig. S1 for coverage). In cyan, the same is shown for the operational model CREG025 instead of PIOMAS over the years 2004-2010. In black scatters, the same is shown for airborne electromagnetic measurements in spring 2011 and 2015 over a small region of the CAA (see Fig. S2 for coverage). In blue scatter, the same in shown for the in-situ CIS Ice Monitoring program at Cambridge Bay, Resolute Bay, Eureka and Alert over the period 1980-2015.
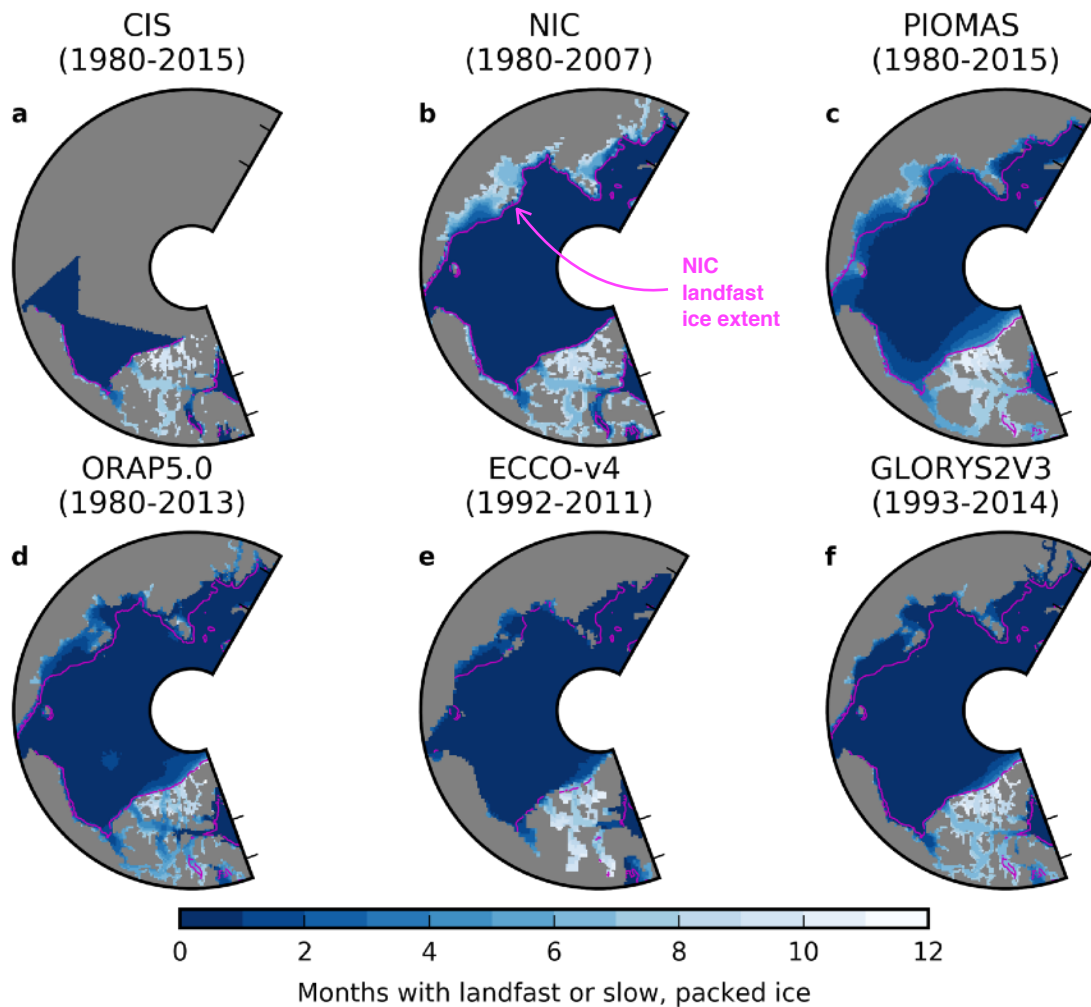
Figure 2. **a**: Historical landfast ice annual duration as reported in the CIS Ice Charts. **b**: Same as **a** but as reported in the National Ice Center (NIC) Ice Charts. **c**: Slow (< 0.864 km day^{-1}), packed (> 85% concentration) ice annual duration as modeled by the assimilation product PIOMAS. **d-f**: Same as **c** but for different ocean reanalyses participating in the ORA-IP. The landfast ice extent, calculated as the 1980-2007 average one-month landfast duration contour from NIC Ice Charts, is shown in magenta.
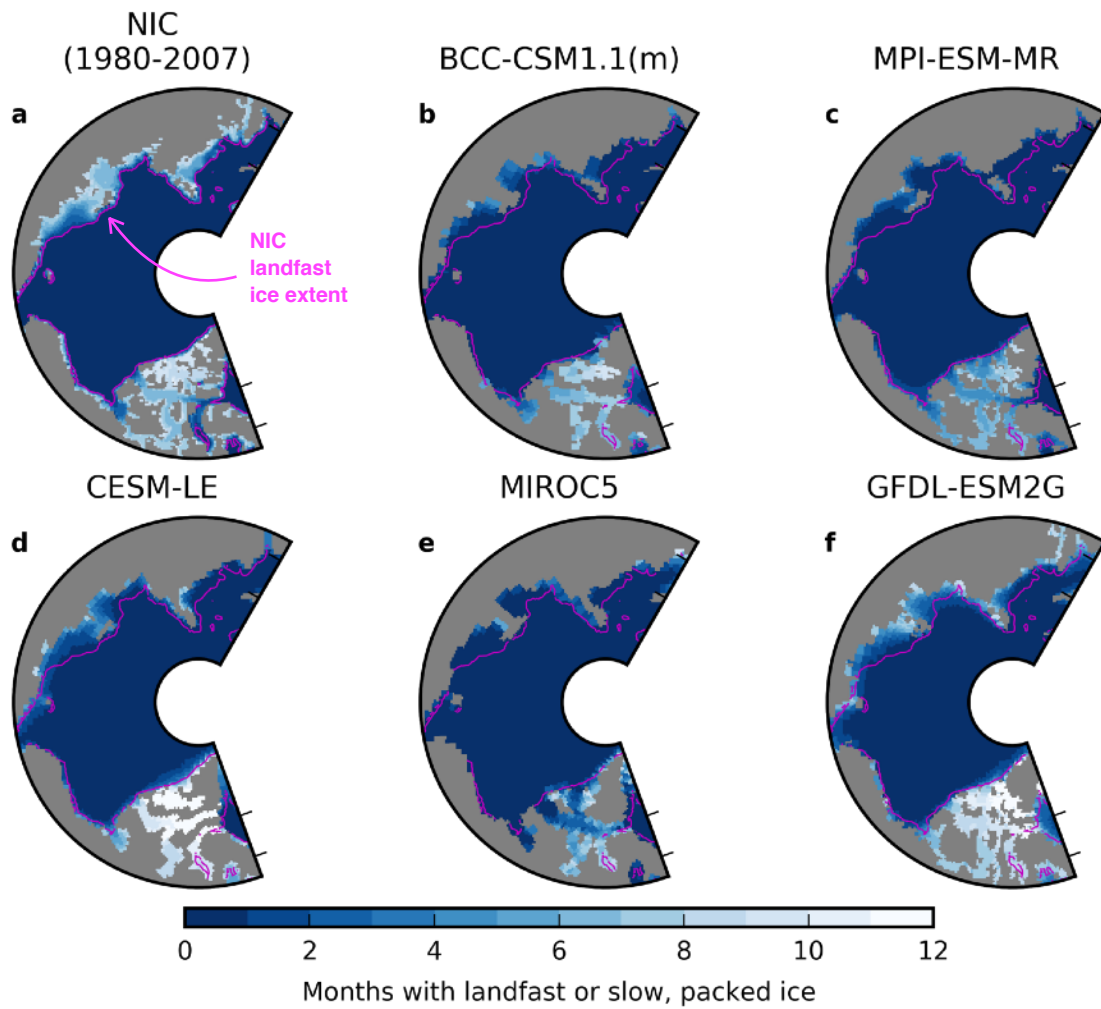
Figure 3. **a**: Same as Figure 2**b**. **b-f**: Same as Figure 2**d-h** except for a subset of simulations from the CMIP5 RCP8.5 scenario over the period 1980-2015.
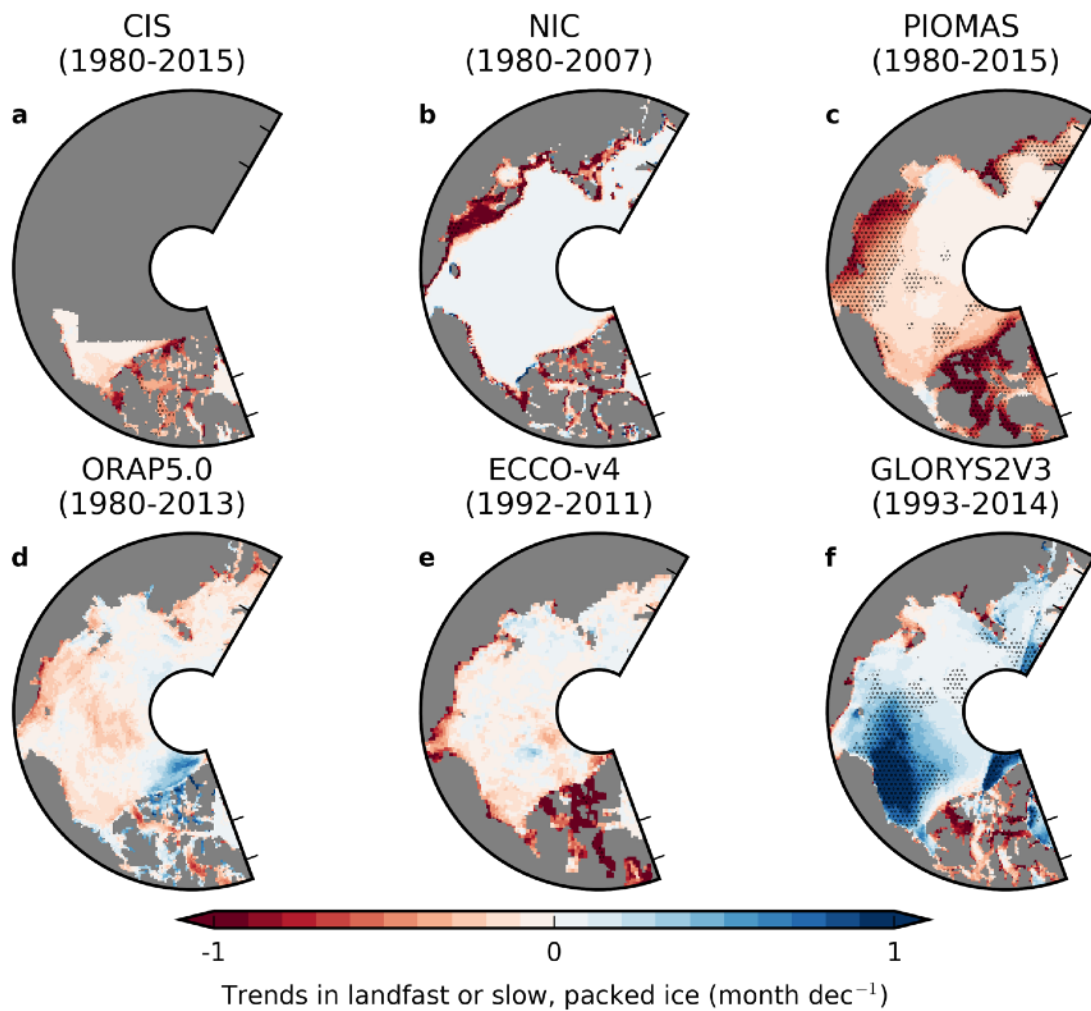
Figure 4. Same as Figure 2 but for the trends in landfast ice duration over the indicated period. Significant trends (p > 0.05) are indicated with stippling. Stippling was removed from some grid points to account for the False Discovery Rate (Wilks, 2006).
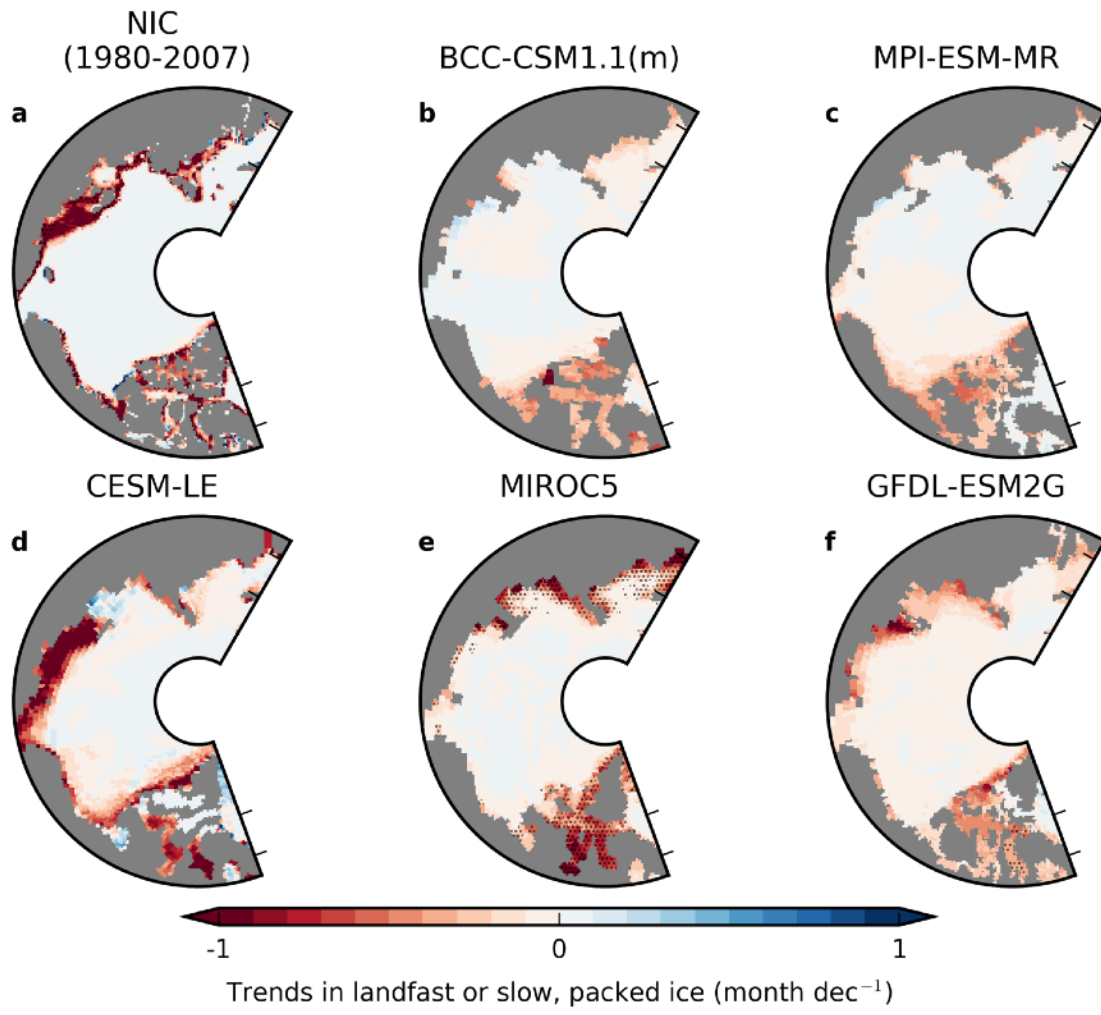
Figure 5. **a:** Same as Figure 5. **b-f:** Same as **a** but the models in Figure 3**b-f** over the period 1980-2015.

Figure 6. **a:** Time series (5 years running-mean) of the fraction of NIC landfast ice extent over the CAA (magenta line in Fig. 2**b**) covered by landfast ice from CIS ice charts for more than the number of months indicated by the line color. **b:** Same as **a** but over the Northwest Passage.
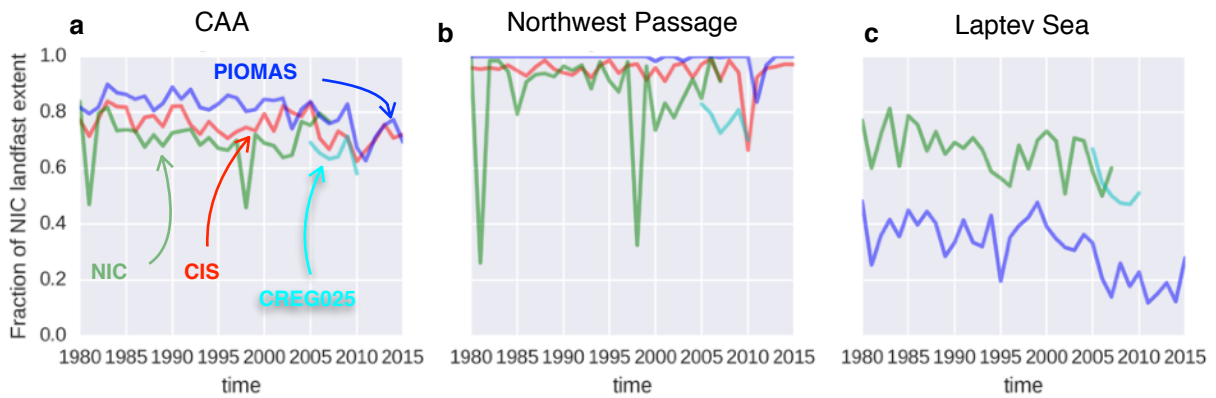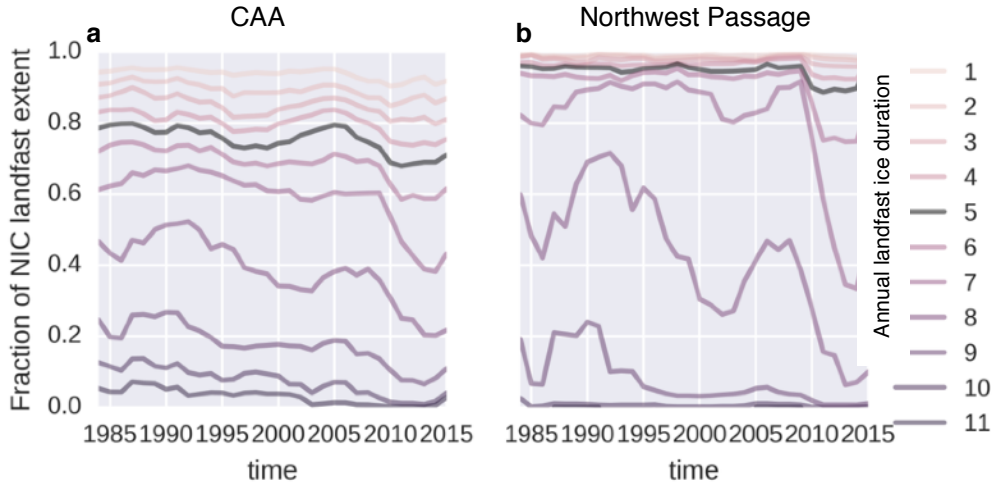
Figure 7. **a:** Time series of the fraction of NIC landfast ice extent (magenta line in Fig. 2**b**) covered by landfast ice (slow, packed ice for PIOMAS and CREG025) with a duration of more than 5 months over the CAA. **b:** Same as **a** but over the Northwest Passage. **c:** Same as **b** but over the Laptev Sea.
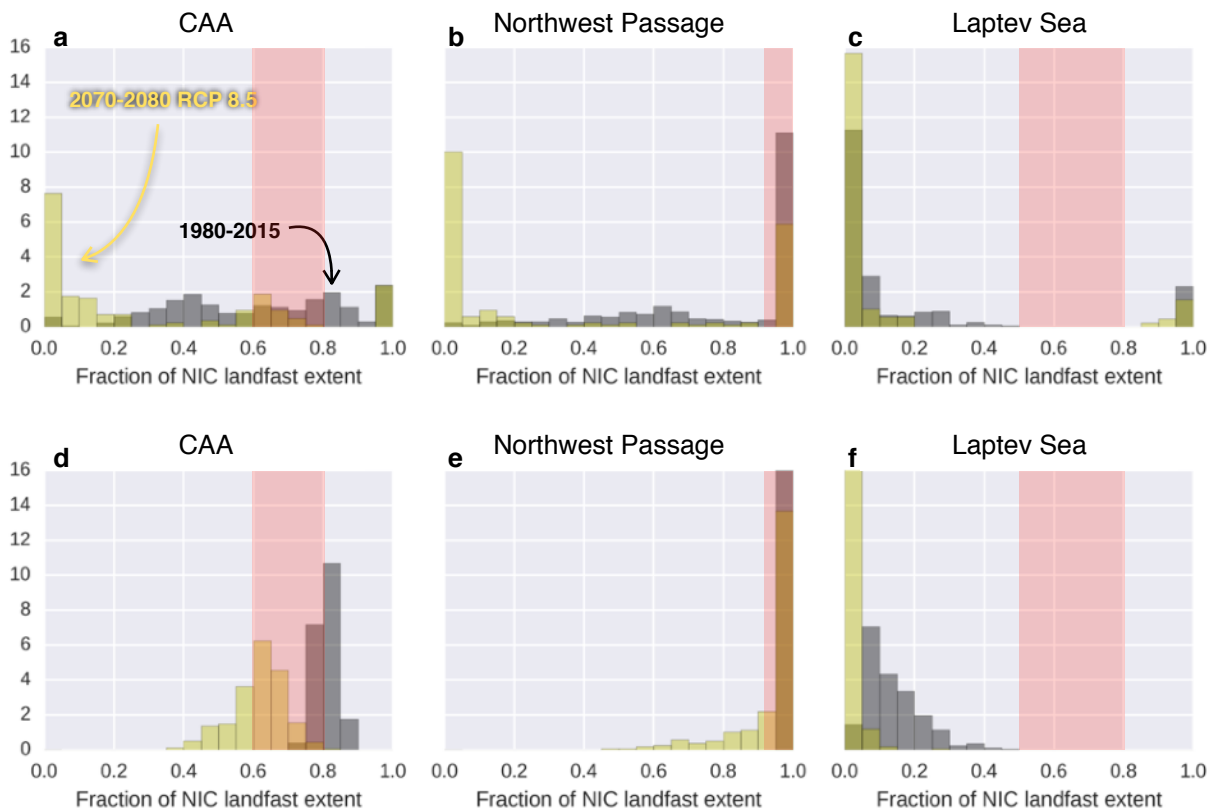
Figure 8. **a:** Distribution (across simulations and years) of the fraction of NIC landfast ice extent (magenta line in Fig. 2**b**) covered by slow, packed ice with a duration of more than 5 months over the CAA for the 1980-2015 period in black and the 2070-2080 period of the RCP 8.5 scenario in yellow. **b:** Same as **a** but over the Northwest Passage. **c:** Same as **b** but over the Laptev Sea. **d-f:** Same as **a-c** but for the CESM-LE. Note that in **e-f** the highest bins go to 21 and 19, respectively. In red shading, we identify the range of observations over the same period, as seen in Figure 7, disregarding PIOMAS in the Laptev Sea.
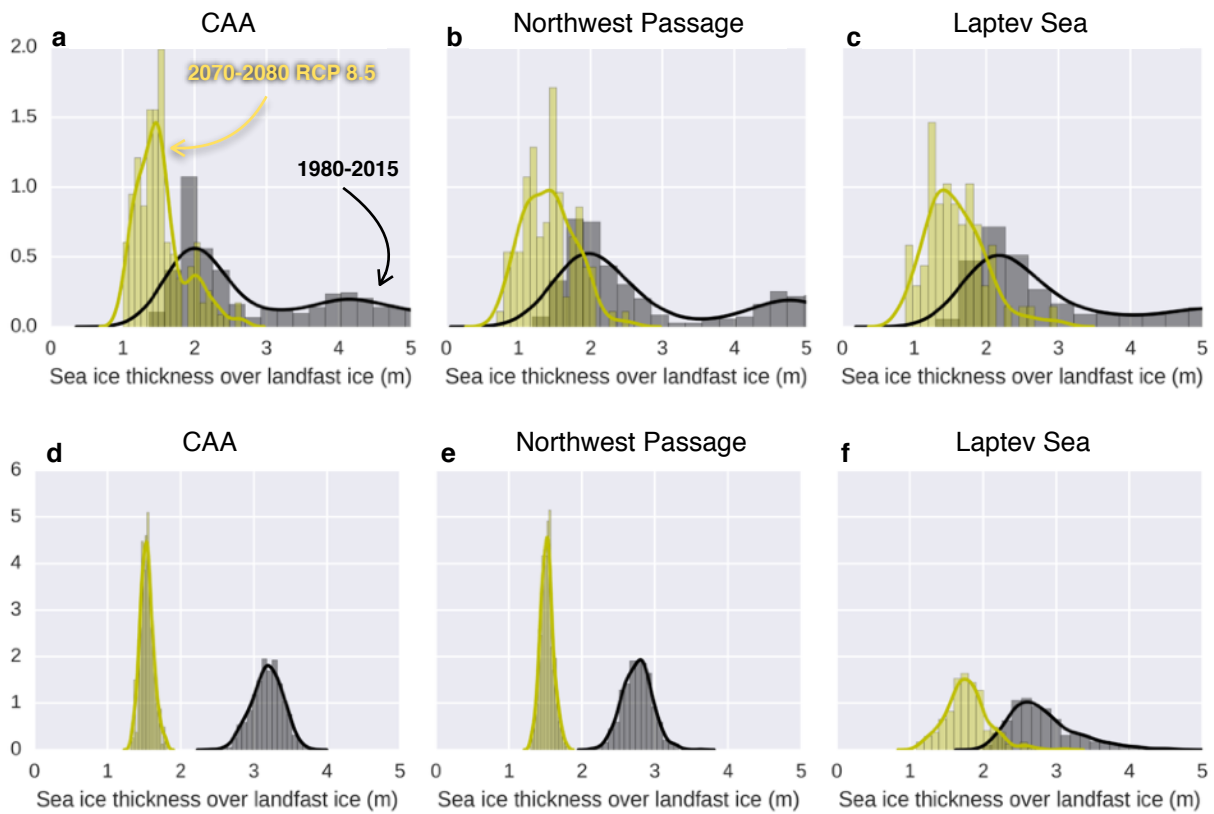
Figure 9. **a:** Distribution (across simulations and years) of the annual maximum ice thickness averaged over landfast ice duration of more than 5 months over the CAA for the 1980-2015 period in black and the 2070-2080 period of the RCP 8.5 scenario in yellow. **b:** Same as **a** but over the Northwest Passage. **c:** Same as **b** but over the Laptev Sea. **d-f:** Same as **a-c** but for the CESM-LE.

CREG025
(2005-2010)

0   2   4   6   8   10   12
Months with landfast or slow, packed ice
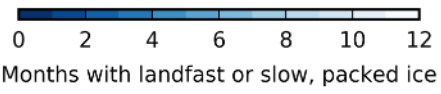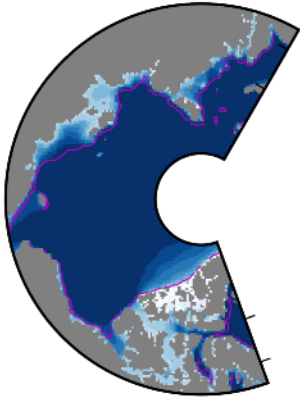
Figure 10. Same as Figure 2**b** but for the CREG025 model.